Lab on a Chip

# Performance Tuning of Microfluidic Flow-Focusing Droplet Generators



| | |
|---|---|
| Journal: | *Lab on a Chip* |
| Manuscript ID | LC-ART-11-2018-001253.R1 |
| Article Type: | Paper |
| Date Submitted by the Author: | 11-Jan-2019 |
| Complete List of Authors: | Lashkaripour, Ali; Boston University, Biomedical Engineering<br>Rodriguez, Christopher; Louisiana Tech University, Department of Cyber Engineering<br>Ortiz, Luis; Boston University, Department of Molecular Biology, Cell Biology & Biochemistry<br>Densmore, Douglas; Boston University, Department of Electrical and Computer Engineering; Biological Design Center |
| | |

Journal Name

ARTICLE TYPE

Cite this: DOI: 10.1039/xxxxxxxxxx

# Performance Tuning of Microfluidic Flow-Focusing Droplet Generators†

Ali Lashkaripour,[a,b] Christopher Rodriguez,[c] Luis Ortiz,[a,d] and Douglas Densmore *[,a,e]

Received Date
Accepted Date

DOI: 10.1039/xxxxxxxxxx

www.rsc.org/journalname

The required step in all droplet-based devices is droplet formation. A droplet generator must deliver an application-specific performance that includes a prescribed droplet size and generation frequency while producing monodisperse droplets. The desired performance is usually reached through several cost- and time-inefficient design iterations. To address this, we take advantage of a low-cost rapid prototyping method and provide a framework that enables researchers to make informed decisions on how to change geometric parameters and flow conditions to tune the performance of a microfluidic flow-focusing droplet generator. We present the primary and secondary parameters necessary for fine-tuning droplet formation over a wide range of capillary numbers and flow rate ratios. Once the key parameters are identified, we demonstrate the effect of geometric parameters and flow conditions on droplet size, generation rate, polydispersity, and generation regime. Using this framework, a wide range of droplet diameters (i.e., $30-400$ $\mu$m) and generation rates ($0.5-800$ Hz.) was achieved.

## 1 Introduction

Droplet-based microfluidic devices enable accurate control over volume and sample concentration while maintaining high-throughput.[1,2] Additionally, a lower cost due to a reduction in reagent consumption[3] makes droplet-based devices suitable alternatives to the current practice in numerous fields, including chemistry,[4] biology,[3] pharmaceutical,[5] and medicine.[6] Microfluidic droplet production can be achieved through T-junction,[7] co-flow,[8] and flow-focusing devices.[9] Flow-focusing geometries are more desirable due to their wide range of droplet size, generation rate and lower coefficient of variation (i.e., *C.V.*) in droplet size when compared to the other geometries.[10,11] However, a complex velocity field and several key parameters defining the geometry have made it challenging to analytically model flow-focusing geometries.[12] On the other hand, a wide variety of aspect ratios causes scaling laws to be too specific to each study, thus, making them not fully representative of the governing physics of flow-focusing droplet formation.[13,14] A droplet generator must produce monodisperse droplets with the droplet size of interest at a certain rate. However, changing geometric parameters and flow conditions to adjust one of the performance metrics (i.e., droplet size or generation rate) results in altering the other performance metric. Therefore, to achieve an application-specific droplet size and production rate, several iterative fine-tuning steps in both geometry and flow conditions are required. Additionally, many applications, such as Fluorescence-activated droplet sorting (FADS), require a narrow size distribution of droplets in order to differentiate droplets based on minute output signal variations measured inside droplets.[15] As a result, monodisperse droplet production is crucial in developing a droplet-based platform. Flow-focusing droplet generators have been shown to deliver monodisperse droplets at low capillary numbers (*Ca.*) when droplets are produced in a highly stable breakup process (i.e., dripping regime).[16] However, due to challenges in controlling the Rayleigh instability in the jetting regime, monodisperse droplet formation is achieved only in a narrow range of operation.[16]

Therefore, the multi-dimensional design space of microfluidic flow-focusing devices has become a challenge rather than an opportunity to gain superior control over the process of droplet formation.[17] As a consequence, designing a flow-focusing microfluidic droplet generator that performs as expected (i.e., application-specific droplet size and generation rate) requires costly and time-consuming design iterations (i.e., both coarse-tuning and fine-tuning steps). There are limited studies that demonstrate how altering each of geometric parameters (i.e., six parameters) changes droplet size, generation rate, polydispersity, and generation regime. Additionally, there is no study that identifies the

[a] *Biological Design Center, 610 Commonwealth Avenue, Boston, MA 02215, USA. E-mail: dougd@bu.edu*
[b] *Boston University Biomedical Engineering Department, Boston, USA.*
[c] *Department of Cyber Engineering, Louisiana Tech University, Ruston, LA.*
[d] *Boston University Department of Molecular Biology, Cell Biology & Biochemistry, Boston, USA.*
[e] *Boston University Department of Electrical and Computer Engineering, Boston, USA.*

† Electronic Supplementary Information (ESI) available: . See DOI: 10.1039/b000000x/

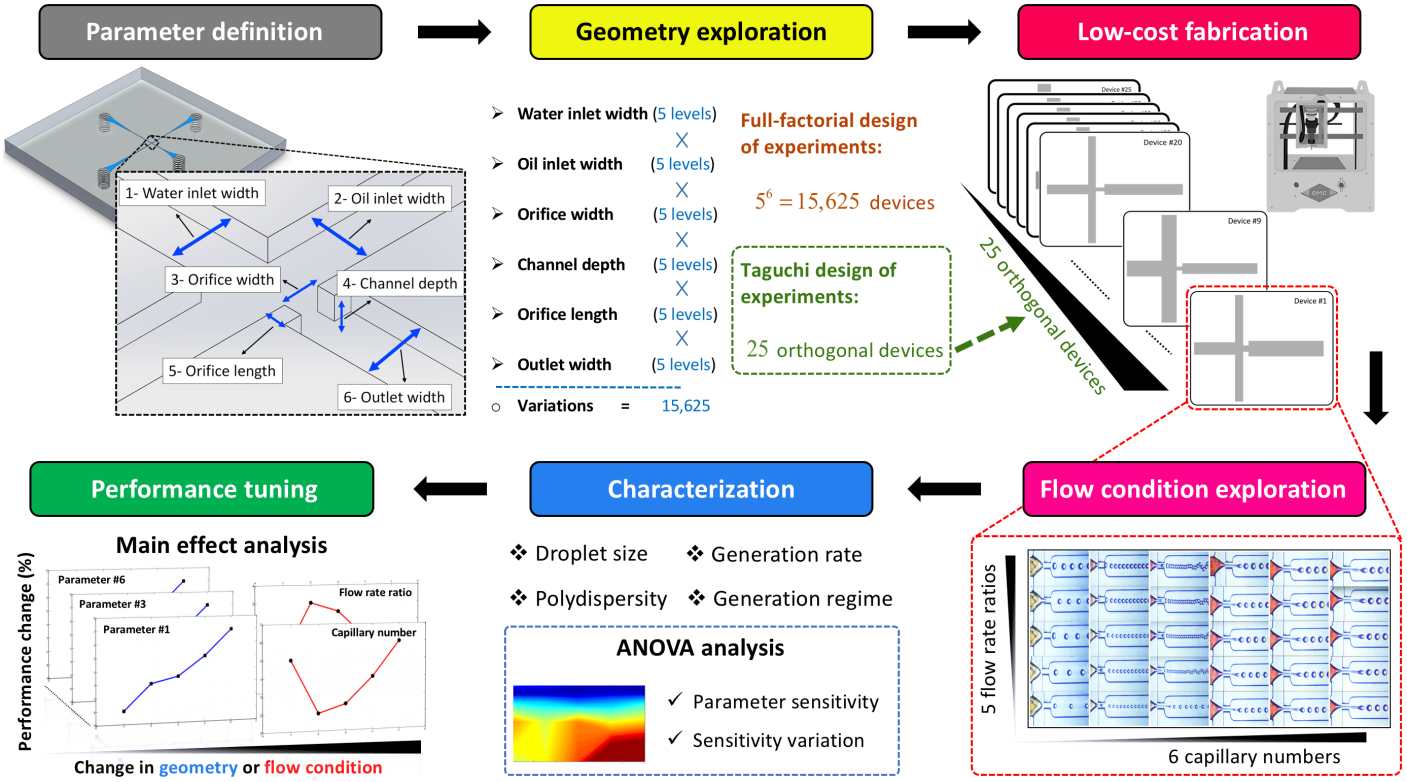


**Fig. 1** In order to tune the performance of a microfluidic droplet generator, dominant parameters and the effect of each parameter on generation rate, droplet diameter, polydispersity, and generation regime at different flow conditions are identified. The effect of six geometric parameters on microfluidic droplet formation is studied by assigning five levels for each parameter. Through Taguchi design of experiments, 25 orthogonal devices are fabricated in a time- and cost-efficient manner using a low-cost desktop micro-mill. Each device is tested at 30 different combinations of capillary numbers and flow rate ratios, to include dripping and jetting droplet formation regimes (i.e., 750 experiments in total). Droplet size and distribution, generation rate and generation regime are documented. By conducting ANOVA analysis, primary (i.e., coarse-tuners) and secondary (i.e., fine-tuners) parameters affecting each performance metric at a given flow condition are introduced. Finally, through the main effect analysis, the performance change induced by changing geometry and flow conditions are reported. Thus, providing an easy framework to fine-tune the performance of droplet generators for a wide range of flow conditions.

primary and the secondary geometric parameters (i.e., coarse-tuners and fine-tuners) for each performance metric; and how the dominance of each geometric parameter changes as the flow conditions vary. This can be attributed to the large design space of flow-focusing devices where six geometric parameters and several fluid and flow properties make the characterization of each parameter, specifically geometric parameters, challenging due to the high fabrication costs. As a result, large design spaces are typically explored using experimentally verified numerical models.[18,19] However, numerical models are prone to inaccuracies, and these inaccuracies are further pronounced in multi-phase flows where capturing the interface between the two phases accurately poses even further challenges.[20] Several low-cost rapid prototyping methods for microfluidics have been introduced recently.[21–23] We exploit a low-cost fabrication method to explore the large design space of microfluidic flow-focusing devices and provide a framework to tune their performance readily.

In this work, we identify the course-tuners and fine-tuners for each performance metric in microfluidic flow-focusing droplet generators. We analyze how the six parameters defining a flow-focusing geometry, affect droplet size, generation rate, polydispersity, and generation regime. A low-cost rapid prototyping method is developed and utilized to explore the large design space of microfluidic droplet generators efficiently. Twenty-five orthogonal devices are fabricated, and each tested at thirty different combinations of capillary number and flow rate ratio (i.e., six capillary numbers and five flow rate ratios) to produce 750 experimental data points. We demonstrate how significant each geometric parameter is in determining each performance metric and illustrate the effect of varying flow conditions on parameter dominance. Once coarse-tuners and fine-tuners for each performance metric are identified, we show how variations in each parameter alter droplet size, generation rate, droplet polydispersity, and generation regime. An overview of the flow of this study is given in Fig. 1.

## 2 Materials and Methods

### 2.1 Flow-focusing geometry

The geometry of a flow-focusing microfluidic droplet generator is shown in Fig. 1. Droplet generation is achieved by flowing the dispersed and the continuous phase through a narrow opening called an orifice. The viscous force exerted by the continuous phase and the sudden reduction in channel width facilitates droplet break-up resulting in fast and monodisperse droplet for-

mation. This geometry is fully defined by a total of six parameters, including orifice width ($Or.$), orifice length ($Or._L$), channel height ($H$), dispersed phase inlet width ($W_d$), continuous phase inlet width ($W_c$), and outlet channel width ($W_o$).[9] Geometric parameters were normalized to the orifice width, as given in Eqs. (1 - 5), so that the findings of this study would be applicable to any flow-focusing geometry regardless of the orifice width.

$$A.R. = \frac{H}{Or.} \tag{1}$$

$$\overline{Or._L} = \frac{Or._L}{Or.} \tag{2}$$

$$\Lambda = \frac{W_o}{Or.} \tag{3}$$

$$\overline{W_d} = \frac{W_d}{Or.} \tag{4}$$

$$\overline{W_c} = \frac{W_c}{Or.} \tag{5}$$

where $A.R.$ is the aspect ratio, $\overline{Or._L}$ is the normalized orifice length, $\Lambda$ in the expansion ratio, $\overline{W_d}$ is the normalized water inlet width, and $\overline{W_c}$ is the normalized oil inlet width. For all the inlets and the outlet width of the microchannels is gradually reduced from the port diameter to the design width. The inlets width were set to be the design width at 10 mm upstream of the orifice to allow for the flow to be fully-developed before entering the orifice. The outlet channel width was kept at the design width up to 5 mm downstream of the orifice, to ensure the design-specific velocity- and pressure-field is achieved.

### 2.2 Design of experiments

A prerequisite to gain fine control over the process of droplet formation is to understand the effect of each geometric parameter on the performance. We studied the impact of geometry on droplet formation by varying the six parameters defining the flow-focusing geometry according to the ranges observed in the literature while considering the fabrications limits.[23] Five different levels were assigned to each parameter in order to create an accurate and representative response of how altering each parameter affects the observed performance. The smallest orifice width was set to be 75 $\mu$m and was increased with steps of 25 $\mu$m for each level, resulting in the largest orifice width of 175 $\mu$m. The aspect ratio (i.e., the channel height normalized by orifice width) and the normalized orifice length were varied from 1 to 3 with steps of 0.5 in between. Expansion ratio (i.e., outlet channel width normalized by orifice width) was increased from 2 to 6 with steps of 1 for each level. Normalized water inlet (i.e., dispersed phase) and normalized oil inlet (i.e., continuous phase) were varied from 2 to 4 with steps of 0.5, as given in Table 1. Given a total of six parameters, each taking five different values, a full-factorial design of experiments requires $5^6 = 15,625$ geometry variations to cover this design-space. However, through the Taguchi orthogonal array design of experiments method,[24] only 25 orthogonal variations (i.e., $L_{25}$ Taguchi orthogonal table) are required to study the same design-space with the minimum possible number of experiments. The $L_{25}$ orthogonal array with the

**Table 1** Flow-focusing geometry is defined by six parameters. In order to accurately clarify the effect of each parameter on droplet formation, five levels are assigned to each parameter. Geometric parameters and their assigned levels are given below. Normalized parameters are divided by the orifice width.

| Parameter | | Levels | | | | |
|---|---|---|---|---|---|---|
| Name | Symbol | #1 | #2 | #3 | #4 | #5 |
| Orifice width ($\mu$m) | Or. | 75 | 100 | 125 | 150 | 175 |
| Aspect ratio | A.R. | 1 | 1.5 | 2 | 2.5 | 3 |
| Expansion ratio | $\Lambda$ | 2 | 3 | 4 | 5 | 6 |
| Normalized water inlet | $\overline{W_d}$ | 2 | 2.5 | 3 | 3.5 | 4 |
| Normalized oil inlet | $\overline{W_c}$ | 2 | 2.5 | 3 | 3.5 | 4 |
| Normalized orifice length | $\overline{Or._L}$ | 1 | 1.5 | 2 | 2.5 | 3 |

Taguchi assigned levels for each parameter is given in Table 2. Each of the 25 orthogonal devices is tested at 30 different combinations of flow conditions, by varying capillary number ($Ca.$) and flow rate ratio ($\Phi$). the capillary number for flow-focusing devices can be defined through Eqs. (6 - 9).[12]

$$Ca. = \frac{\mu_c u_c}{\sigma} \tag{6}$$

where $\mu_c$, $u_c$ are the dynamic viscosity and the velocity of the continuous phase, respectively. $\sigma$ is the surface tension between the dispersed and the continuous phase. Through the definition of the centerline velocity gradient, the velocity term can be rewritten as given in Eq. (7).

$$Ca. = \frac{\mu_c G \cdot a}{\sigma} \tag{7}$$

where $G$ is the strain rate, $a$ is the undeformed droplet radius (i.e., the half width of the dispersed phase inlet in flow-focusing geometry). The strain rate can be estimated by the gradient of the average velocity of the continuous phase between the orifice and the upstream continuous phase inlet, as given Eq. (8).

$$Ca. = \frac{\mu_c a}{\sigma} \cdot \frac{\Delta u}{\Delta z} \tag{8}$$

where $\Delta u$ is the difference between the average velocity of the continuous phase at the inlet and the orifice, and $\Delta z$ is the distance between the velocity centerline of the continuous phase inlet and the orifice entrance which is the equivalent of the half width of the continuous phase inlet. According to this, capillary number can be calculated using Anna and Mayer definition[25] as given in Eq. (9).

$$Ca. = \frac{\mu_c W_d Q_c}{\sigma H \cdot W_c} \left[ \frac{1}{Or.} - \frac{1}{2 \cdot W_c} \right] \tag{9}$$

In this study, flow rate ratio is defined by the ratio of the continuous phase (i.e., mineral oil) flow rate and the dispersed phase (i.e., water) flow rate as given in Eq. (10) .

$$\Phi = \frac{Q_c}{Q_d} \tag{10}$$

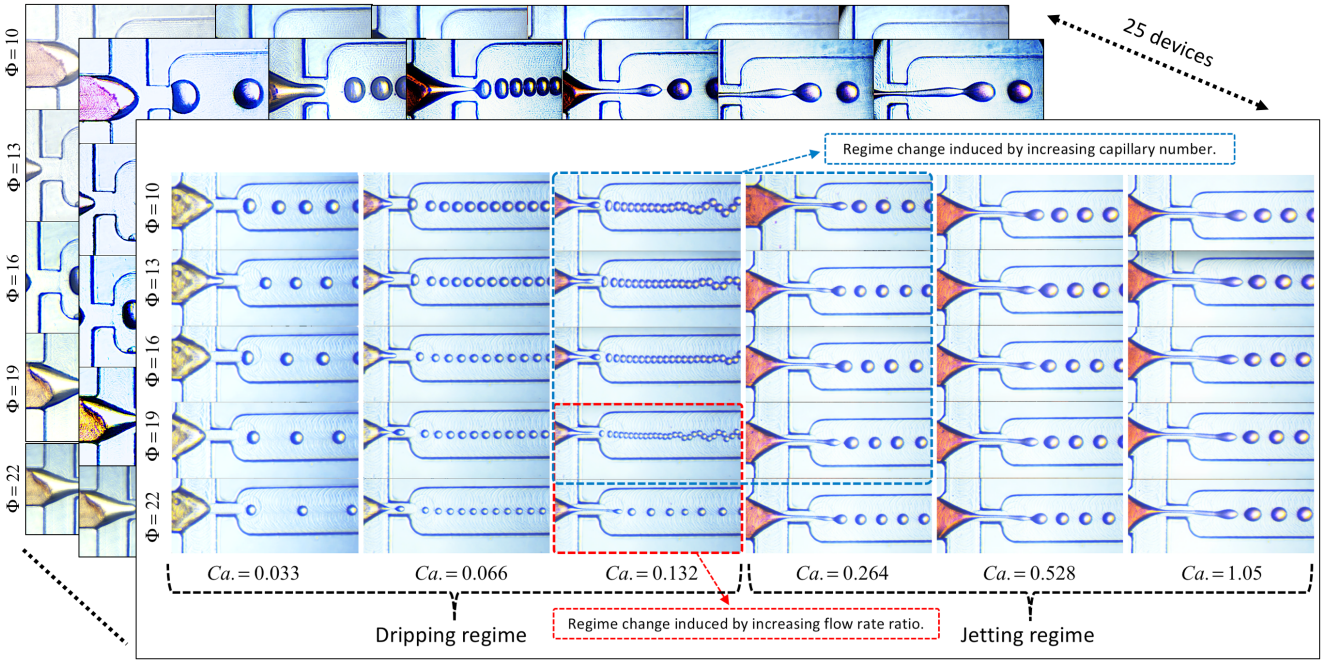


**Fig. 2** Each device is tested at low to high capillary numbers (i.e., $Ca. = 0.03 - 1$) to cover a relatively large range of droplet generation rates. Additionally, to deliver a biologically relevant droplet size, at each capillary number flow rate ratio was varied from $\Phi = 10$ to 22. An example of snapshots taken from a single device tested at different flow conditions is shown. Each device is tested at 6 different capillary numbers and 5 different flow rate ratios (i.e., a total of 30 flow conditions). Given a total of 25 orthogonal devices, 750 experiments are conducted and for each experiment droplet diameter, generation rate, droplet polydispersity, and generation regime are recorded.

**Table 2** 25 orthogonal devices proposed by Taguchi design of experiments method are given below. A total of six geometric parameters defining the flow-focusing geometry and considering 5 levels for each parameter a full-factorial design of experiments would result in $5^6 = 15,625$ devices. However, this design space can be studied using a $L_{25}$ Taguchi orthogonal table with a minimum of 25 devices.

| Device | | Geometric parameters | | | | |
|---|---|---|---|---|---|---|
| No. | Or. ($\mu$m) | A.R. | $\Lambda$ | $\overline{W_d}$ | $\overline{W_c}$ | $\overline{Or._L}$ |
| #1 | 75 | 1 | 2 | 2 | 2 | 1 |
| #2 | 75 | 1.5 | 3 | 2.5 | 2.5 | 1.5 |
| #3 | 75 | 2 | 4 | 3 | 3 | 2 |
| #4 | 75 | 2.5 | 5 | 3.5 | 3.5 | 2.5 |
| #5 | 75 | 3 | 6 | 4 | 4 | 3 |
| #6 | 100 | 1 | 3 | 3.5 | 4 | 2 |
| #7 | 100 | 1.5 | 4 | 4 | 2 | 2.5 |
| #8 | 100 | 2 | 5 | 2 | 2.5 | 3 |
| #9 | 100 | 2.5 | 6 | 2.5 | 3 | 1 |
| #10 | 100 | 3 | 2 | 3 | 3.5 | 1.5 |
| #11 | 125 | 1 | 4 | 2.5 | 3.5 | 3 |
| #12 | 125 | 1.5 | 5 | 3 | 4 | 1 |
| #13 | 125 | 2 | 6 | 3.5 | 2 | 1.5 |
| #14 | 125 | 2.5 | 2 | 4 | 2.5 | 2 |
| #15 | 125 | 3 | 3 | 2 | 3 | 2.5 |
| #16 | 150 | 1 | 5 | 4 | 3 | 1.5 |
| #17 | 150 | 1.5 | 6 | 2 | 3.5 | 2 |
| #18 | 150 | 2 | 2 | 2.5 | 4 | 2.5 |
| #19 | 150 | 2.5 | 3 | 3 | 2 | 3 |
| #20 | 150 | 3 | 4 | 3.5 | 2.5 | 1 |
| #21 | 175 | 1 | 6 | 3 | 2.5 | 2.5 |
| #22 | 175 | 1.5 | 2 | 3.5 | 3 | 3 |
| #23 | 175 | 2 | 3 | 4 | 3.5 | 1 |
| #24 | 175 | 2.5 | 4 | 2 | 4 | 1.5 |
| #25 | 175 | 3 | 5 | 2.5 | 2 | 2 |

As shown in Fig. 2, each device is tested at six different capillary numbers and five different flow rate ratios. Capillary number was varied from 0.033 to 1.057 to include multiple data points of both dripping and jetting regimes (i.e., 361 data points for the dripping regime and 389 data points for the jetting regime).[12] Given the smallest orifice width of 75 $\mu$m in this study, flow rate ratio was varied from 10 to 22 to produce droplets smaller than the orifice width to be relevant in applications where a droplet diameter smaller than 75 $\mu$m is desired. Each device is tested at 30 different flow conditions. Therefore, having 25 devices, overall a total of 750 experiments were conducted and droplet diameter, generation rate, polydispersity, and generation regime were recorded.

### 2.3 Low-cost rapid prototyping

Several cost-effective methods to fabricate microfluidic devices such as low-cost photolithography and cyclic olefin copolymer (i.e., COC) casting have been introduced recently.[22,26] Although these methods offer significant cost reduction in comparison to standard photolithography, they often require extra steps of soft-lithography, chemical/thermal bonding, and surface treatment for droplet-based applications in comparison to direct micro-milling of polycarbonate-based devices, resulting in a higher cost and/or longer time of fabrication.[27,28] In order to rapidly prototype microfluidic devices in a time- and cost-efficient manner we exploited a fabrication method we previously developed.[23] A low-cost (< $3200) desktop CNC micro-mill (Othermill Pro, Bantam tools, CA, USA) was used to ablate micro-channels from a polycarbonate substrate with a thickness of 5.5 mm. Designs were created in SolidWorks (Dassault Systèmes) and .STEP

files were loaded in Fusion 360 (Autodesk) to create the milling paths (.GCODE). Different endmills with cutting diameters varying from 75 $\mu$m to 3.175 mm (Performance micro tool, and Bantam tools endmills) were used. Using this method, the smallest feature of 75 $\mu$m can be milled out, with an accuracy of 10 $\mu$m for the orifice (i.e., single-pass milling path) and 25 $\mu$m for other channels (i.e., multiple-passes milling path) in the X-Y plane, as further explained in supplementary information section S. 1. Channel depth was verified using an electronic indicator, with a resolution of 10 $\mu$m (Fowler, MA, USA). Through this method, each device was fabricated in less than 1 hour and cost less than \$10.[23] Device layers were cleaned before assembly with a mixture of DI water and rubbing alcohol in an ultrasonic cleaner (X-tronic, NE, USA) at 40°C. A thin (i.e., $\approx$ 250 $\mu$m) Polydimethylsiloxane (PDMS) layer was sandwiched between the flow and control layer to seal the chip by applying a vacuum using a desiccator. To increase the sealing pressure, two layers of pressure distributors milled out of polycarbonate were used to hold down the flow and control layer using clamps as shown in Fig. 3. More details on the fabrication and assembly process are provided in supplementary information section S. 1.

### 2.4 Experimental setup

Syringe pumps (New Era, NY, USA) were used to introduce fluids inside the microfluidic chip. A 50 cm long flexible PVC tubing (McMaster-Carr, NJ, USA) with an inside diameter of 1.6 *mm* (i.e., 1/16 *in*) was used as a low-pass filter to dampen small fluctuations in flow rate naturally induced by syringe pumps to achieve monodisperse droplets.[29] A high-speed camera (IDT XStream, NJ, USA) was mounted on a stereo-microscope (AmScope, CA, USA) to capture videos of droplet generation, with up to 10,000 frames per second, depending on the speed of the experiment. A high-powered high-intensity LED pulse light source delivering 18000 Lumens (Expert Digital Imaging, MA, USA) was used and was placed under the microfluidic device. Mineral oil with a viscosity of 57.2 mPa.s and density of 0.857 kg/m$^3$ was used as the continuous phase. 5% volumetric Span 80 (Sigma-Aldrich) surfactant was added to the mineral oil in order to reduce the surface tension to 0.005 N/m and increase droplet stability.[30] DI water was used as the dispersed phase, with food color added to improve experimental visualization. All fluids were filtered before introduction to the microfluidic device using a Steriflip Polyvinylidene Fluoride (i.e., PVDF) filter (Sigma-Aldrich) with a pore size of 0.45 $\mu$m.

### 2.5 Image processing

A custom-made image-processing software was developed specifically for microfluidic flow-focusing devices. To measure the generation rate the average pixel intensity over a bounding box for every frame in the video was recorded. As a droplet passes through the bounding box, the average pixel intensity would increase. By measuring the frequency of the pixel intensity oscillations, droplet generation rate was calculated. Droplet diameter was extracted through finding the droplet contour using the OpenCV built-in Canny edge detection package.[31,32] Sklansky's algorithm was then implemented to find the convex hull over the contours to report the droplet diameter.[33] This tool is called $\mu$-DROP and is available as an open-access software at: `https://github.com/CIDARLAB/uDrop-Generation`

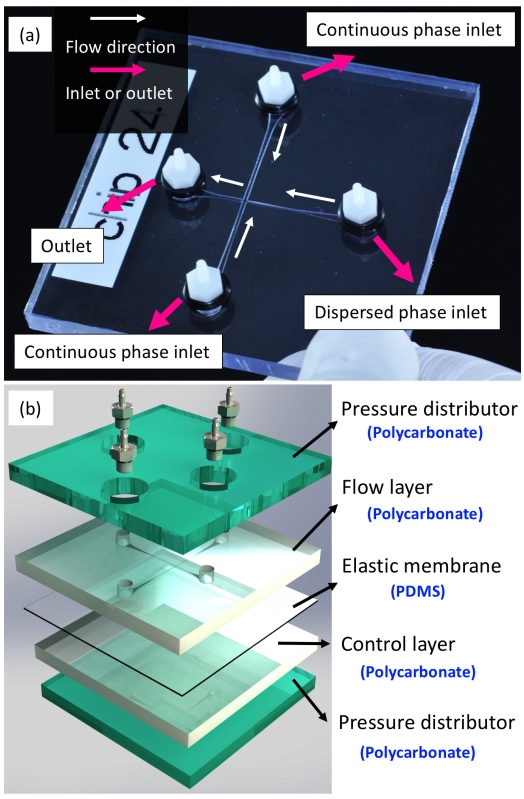


**Fig. 3** (a) Flow layer of a microfluidic droplet generator, milled out of polycarbonate using a low-cost desktop CNC micro-mill in less than 1 hour while costing less than \$10. (b) Each device consists of five layers. The flow and the control layer are milled out of polycarbonate and sealed using a thin layer of PDMS (i.e., $\approx$ 250 $\mu$m). Two layers of pressure distributors (rendered in green) are milled out of polycarbonate and clamped down to deliver a uniform and reversible seal throughout the device. More information on fabrication and assembly of the microfluidic devices is provided in the supplementary information section S. 1.

### 2.6 ANOVA analysis

We exploited ANOVA method to determine the sensitivity of each performance metric to the geometric parameters at a given flow condition. ANOVA method assigns an F-value to each parameter by comparing the variances between the groups and the variance within each group. According to the ANOVA method, the sum of squares of between the groups (i.e., $SS_B$) is calculated using Eq. (11).

$$SS_B = \sum_1^k n_i \left(\overline{X_i} - \overline{X}\right)^2 \tag{11}$$

where $k$ is the number of groups, $n_i$ is the number of observations in each group, $X_i$ is the mean of the $i_{th}$ group, and $\overline{X}$ represents the overall mean. Sum of squares within the groups (i.e., $SS_W$) is given by Eq.(12)

$$SS_W = \sum_1^k (n_i - 1){s_i}^2 \tag{12}$$

where $s_i$ is the standard deviation of the $i_{th}$ group, thus, ${s_i}^2$ is the variance of the $i_{th}$ group. Mean square between, and within the groups can be calculated using Eq.(13), and Eq.(14), respectively.

$$MS_B = \frac{SS_B}{k-1} \tag{13}$$

$$MS_W = \frac{SS_W}{n-k} \tag{14}$$

where $n$ is the total number of observations given by Eq. (15)

$$n = n_1 + n_2 + \cdots + n_k \tag{15}$$

F-value is then calculated using Eq. (16).

$$F = \frac{MS_B}{MS_W} \tag{16}$$

A larger F-value ($F > 1$ and higher) represents a more significant parameter. If $F \leq 1$, the parameter of interest has no significant effect on the observation.[34]

### 2.7 Main effect analysis

Main effect analysis provides insight into how independent parameters affect a dependent variable.[35] Main effect plots display the average response recorded for each level of a categorical parameter in all the experiments. Therefore, main effect analysis determines how altering a single parameter changes the response of a system while averaging over the other parameters. Thus, main effect plots are simple and powerful tools to study system response dependency on a specific parameter in a system with multiple effective parameters.[36] In this study, main effect analysis was used to determine how changing geometric parameters and flow conditions affect the performance of droplet generation.

## 3 Results

In order to tune the performance of microfluidic droplet generators, primary (i.e., coarse-tuners) and secondary (i.e., fine-tuners) parameters should be differentiated from parameters with no considerable effect. To achieve this, we obtained 750 experimental data points (i.e., 25 orthogonal devices, tested and 30 unique flow conditions) that relate six geometric parameters, capillary number, and flow rate ratio to the observed performance (i.e., droplet diameter, generation rate, polydispersity, and generation regime). We used analysis of variance (i.e., ANOVA) method to establish how sensitive each performance metric is to the geometric parameters. ANOVA analysis outputs an F-value for each parameter at a given flow condition. A higher F-value reflects a more significant and dominant parameter, at a given flow condition. Additionally, by varying the flow conditions (i.e., capillary number and flow rate ratio), we studied how the significance of each parameter varies for 30 different flow conditions, that include both dripping and jetting droplet formation regimes. Therefore, by comparing the performance of the 25 devices at the same flow condition, using ANOVA method, we obtained an F-value for each geometric parameter at a given flow condition. We repeated this for all of the 30 flow conditions while considering generation rate, droplet diameter, polydispersity, and generation regime, separately (i.e., 30 ANOVA analysis for each performance metric and 120 ANOVA analyses in total). It should be mentioned that orifice length had the least significance in defining the performance (see Fig. S. 11 in the supplementary infromation), therefore, we generated four heat-maps that include the five most significant geometric parameters (i.e., Fig. 4. a, Fig. 5. a, Fig. 6. a, and Fig. 7. a) for each performance metric by assigning a color to each F-value. A warmer region on the heat-map indicates a higher sensitivity of the performance metric of interest to a specific geometric parameter. Therefore, regions in red are the coarse-tuners in the sense that altering that geometric parameter will result in a significant change in the performance metric. Regions in yellow and green are the fine-tuners, meaning that altering that geometric parameter will lead to a less significant change in performance. The blue regions indicate that varying a geometric parameter at a constant flow condition results in a negligible change in performance. Once, the sensitivity of performance to each geometric parameter is established, the main effect analysis is carried out to determine how varying each of the parameters (i.e., both geometric parameters and flow conditions) changes the performance of droplet generation. We presented the analysis results for tuning generation rate, droplet diameter, polydispersity, and regime are given in section 3.1, 3.2, 3.3, and 3.4, respectively.

### 3.1 Tuning generation rate

Results of ANOVA analysis (i.e., parameter sensitivity) for droplet generation rate at different flow conditions are shown in Fig. 4. (a). According to ANOVA, at low capillary numbers (i.e., $Ca. = 0.03 - 0.07$) normalized water inlet width and normalized oil inlet width were the dominant parameters in determining droplet generation frequency. At moderate capillary numbers (i.e., $Ca. = 0.1 - 0.3$), aspect ratio and expansion ratio became the most influential parameters in tuning generation rate. Aspect ratio plays a dominant role at these capillary numbers due to its effect in determining the generation regime. A higher aspect ratio will lead to a regime change at a lower capillary number where a sudden reduction of generation rate is observed (as will be discussed in 3.4). At the high capillary numbers (i.e., $Ca. > 0.5$ or jetting regime), the expansion ratio was observed to be the primary parameter affecting the generation rate. Using Fig. 4. (a), researchers can identify the coarse- and fine-tuners of generation rate for a given flow condition, and change them accordingly to control droplet generation rate. In order to establish if changing a parameter results in a decrease or an increase in generation rate, main effect analysis was conduced. The main effect plots for generation rate are given in Fig. 4. (c). The results of the main effect analysis were normalized by the average generation rate observed in the 750 experiments (i.e., 111.8 Hz.) in order to translate variations in generation rate to a percent change in the observed generation frequency. It can be concluded that increasing orifice width, aspect ratio, expansion ratio, and water inlet width result in a reduced generation rate. As further explained in the supplementary information sections S. 2. and S. 3., expansion ratio only affects generation rate when droplets are formed at the jetting the regime. On the other hand, we demon-

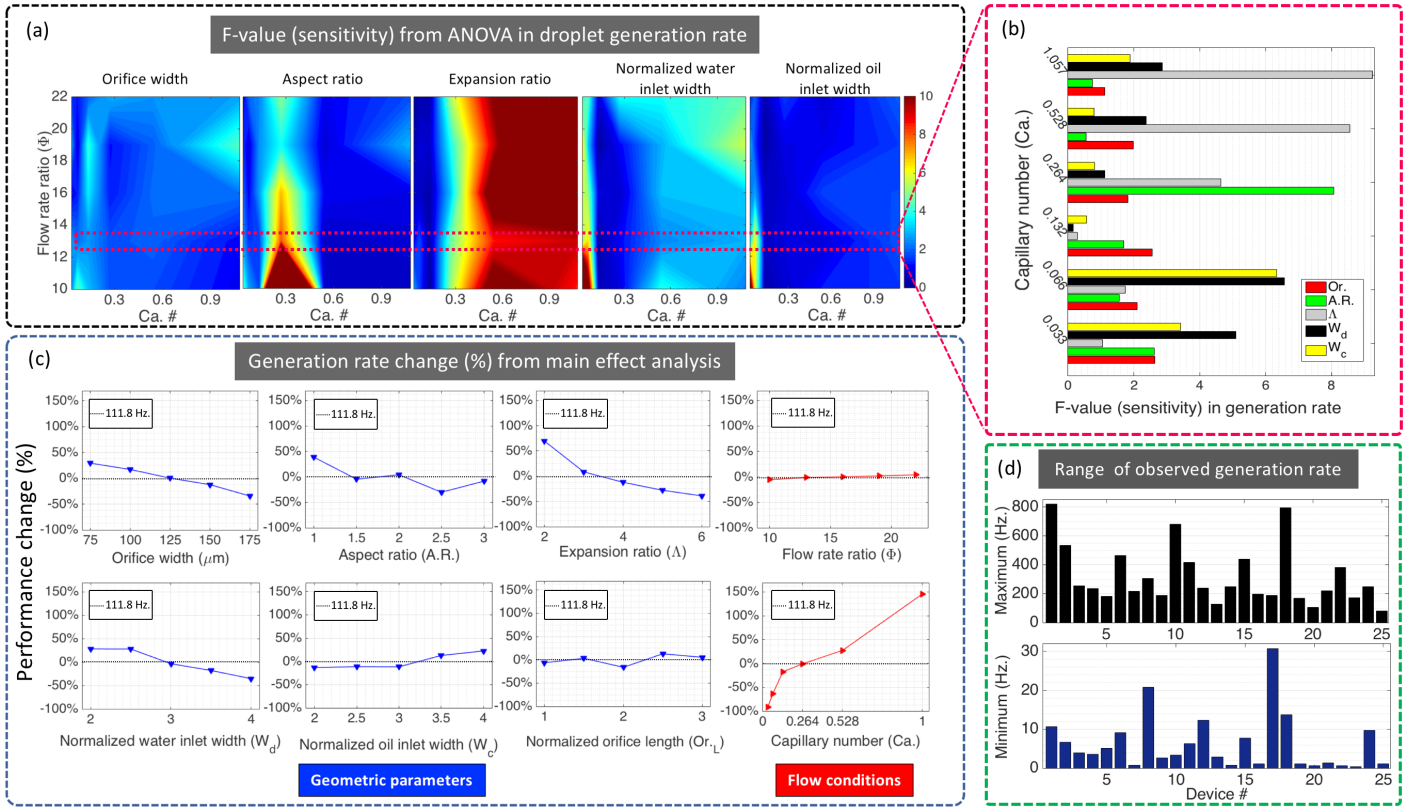


**Fig. 4** Researchers can use this framework to identify the primary and secondary parameters in generation rate at a given flow condition and then fine-tune geometry and flow conditions to achieve the desired generation rate. (a) A heat-map of sensitivity variation of generation rate to each geometric parameter at different flow conditions. At low capillary numbers (i.e., $Ca. =$ 0.033 - 0.066) water and oil inlet width are the dominant parameters. At medium capillary numbers ($Ca. = 0.132 - 0.264$) aspect ratio becomes the significant factor. At high capillary numbers ($Ca. > 0.264$) expansion ratio is the definitive factor in generation rate. (b) A slice of the heat-map shown in (a) at a constant flow rate ratio (i.e., $\Phi = 13$) that further clarifies the generation rate sensitivity variations at low capillary numbers relative to medium and high capillary numbers. (c) Main effect plots demonstrating how variations in parameters affect generation rate for both geometric parameters (blue) and flow conditions (red). Each plot shows how altering a parameter results in a percent deviation from the average observed generation rate (i.e., 111.8 Hz.). (d) Maximum and minimum generation rates observed for each device are given. Researchers can use this range alongside Table S. 1 in the supplementary information to choose a device and further adjust its parameters using information provided in (a) and (c) to achieve a generation rate of interest. More information on performance tuning of droplet generation based on the observed generation regime is provided in supplementary information sections S. 2. and S. 3.

strated that increasing oil inlet width and capillary number led to a higher generation rate. It was also shown that orifice length and flow rate ratio have a negligible effect on generation rate. Still, the flow rate ratio was observed to result in a slight increase in the generation rate. An almost linear dependence of generation rate on orifice width, aspect ratio, and expansion ratio was observed. As a result, the generation rate can be readily tuned by changing these three geometric parameters, while keeping other parameters and flow conditions constant. The capillary number was the most influential parameter in determining the frequency of droplet formation. The minimum and maximum generation rate observed for each device is given in Fig. 4. (d). Researchers can use the observed range of each device from Fig.4. (d) and fine tune the device of interest using information provided in Fig. 4. (a) & (c) to achieve the desired generation rate. Additionally, in order to tune the generation rate more accurately based on the observed droplet formation regime Fig. S. 5 and Fig. S. 7 of the supplementary information can be used for dripping regime and jetting regime, respectively.

### 3.2 Tuning droplet size

The significance of each geometric parameter (i.e., F-values obtained from ANOVA) in determining the droplet diameter at different flow conditions are shown in Fig. 5. (a). The orifice width was observed to be the key parameter in dictating the droplet size regardless of the flow condition. We showed that aside from the orifice width, aspect ratio and expansion ratio were also important in regulating the droplet diameter. The sensitivity of droplet size to aspect ratio and expansion ratio was more pronounced at medium to high flow rate ratios, where a geometry dependent generation regime change could occur (i.e., from dripping to jetting) that results in a sudden increase in droplet diameter. It can be concluded that among the geometric parameters orifice width is the coarse-tuner and aspect ratio and expansion ratio are the fine-tuners of droplet diameter. By using the main effect analysis, the roles of the geometric parameters, capillary number, and flow rate ratio on droplet size were studied. The main effect analysis results for droplet diameter are given in Figure 5. (c). The main effect analysis plots were normalized by the average droplet di-

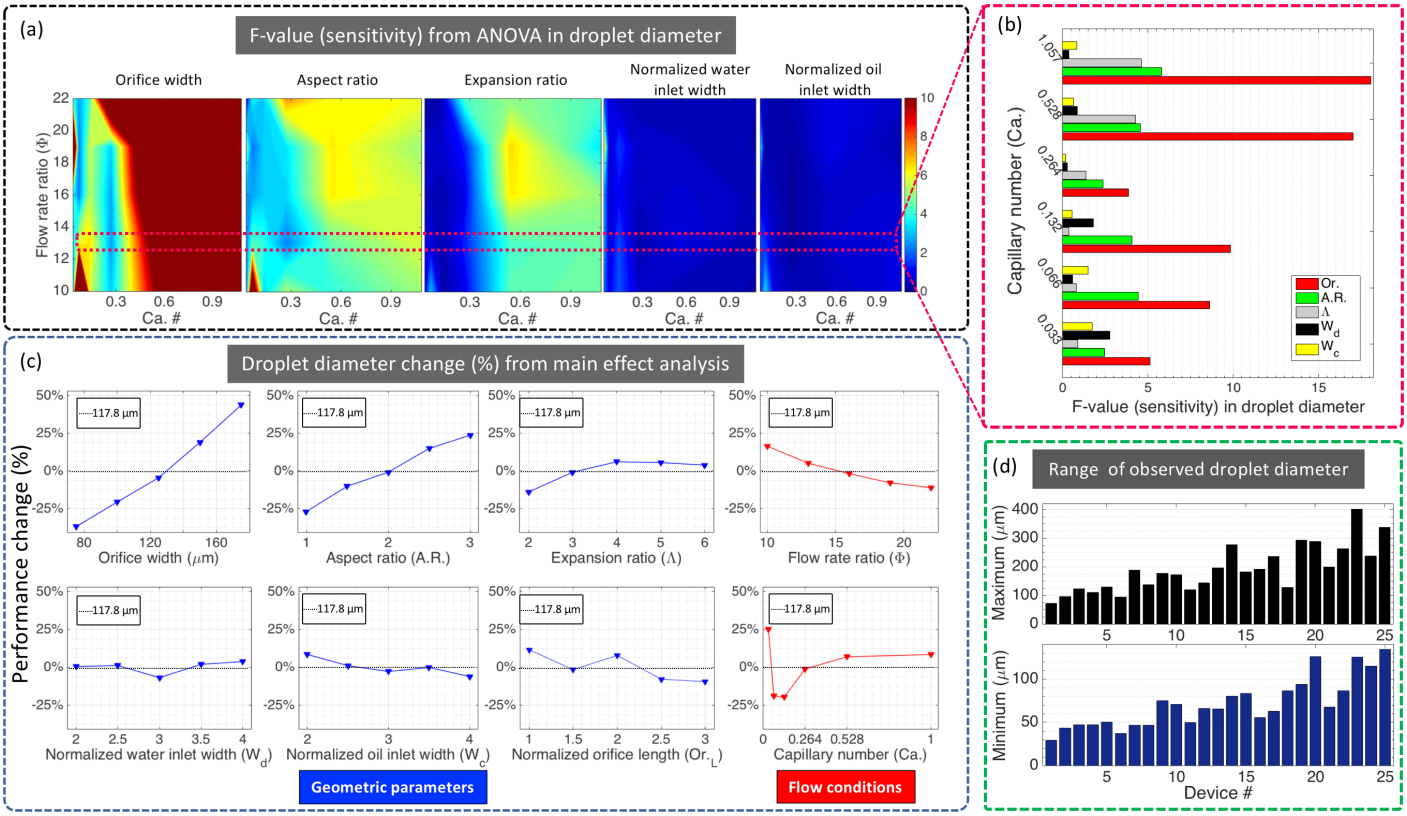


**Fig. 5** The framework that researchers can use to identify the primary and secondary parameters in determining the droplet diameter at a given flow condition and fine-tune geometry and flow conditions to achieve the desired droplet size. (a) A heat-map of sensitivity variation of droplet size to each geometric parameter at different flow conditions. As expected, the orifice width is the dominant parameter in defining droplet size. Aspect ratio is the secondary parameter in determining the droplet size. At high capillary numbers or jetting regime ($Ca. > 0.528$) expansion ratio also becomes important in regulating droplet size. (b) A slice of the heat-map shown in (a) at a constant flow rate ratio (i.e., $\Phi = 13$) that further clarifies the droplet size sensitivity variations at low capillary numbers relative to medium and high capillary numbers. (c) Main effect plots demonstrating how variations in parameters affect droplet diameter for both geometric parameters (blue) and flow conditions (red). Each plot shows how altering a parameter results in a percent deviation from the average observed droplet diameter (i.e., 117.8 $\mu$m.) (d) Maximum and minimum droplet diameters observed for each device are given. Researchers can use this range alongside with Table S. 1 in the supplementary information to pcik a device and further adjust its parameters using information provided in (a) and (c) to generate a droplet with a diameter of interest. More information on performance tuning of droplet generation based on the observed generation regime is provided in supplementary information sections S. 2. and S. 3.

ameter observed in the 750 experiments (i.e., 117.8 $\mu$m.) in order to translate alterations in droplet size to a percent change in the observed droplet diameter. We demonstrated an increase in the orifice width, aspect ratio, and expansion ratio results in larger droplets. However, altering expansion ratio was observed to be more effective on changing droplet diameter when droplet formation occurred at the jetting regime in comparison to dripping regime as further shown in Fig. S. 4 and Fig. S. 6. On the other hand, a larger oil inlet, orifice length, and flow rate ratio results in a reduced droplet size. We observed that water inlet width had a negligible effect on droplet size. Orifice width and aspect ratio showed an almost linear relation with droplet diameter. Therefore, while keeping all the other geometric parameters, capillary number and flow rate ratio constant, flow-focusing droplet generators can be readily tuned by changing orifice width (i.e., as the coarse-tuner) and aspect ratio and expansion ratio (i.e., as the fine-tuners) to achieve a desirable droplet diameter. Also, it was shown that increasing capillary number within the dripping regime (i.e., $Ca. < 0.14$) resulted in smaller droplets. However, further increasing the capillary number induced a regime change at $Ca. = 0.15 - 0.3$ (i.e., from dripping to jetting) that resulted in a sudden increase in droplet size. Increasing the capillary number after this point (i.e., $Ca. > 0.4$) had almost no effect on droplet diameter. The minimum and the maximum observed droplet diameter for each device are given in Fig. 5. (d). Researchers can use the observed range of droplet diameter and choose a device according to their desired performance and fine tune the device of interest using information provided in Fig. 5. (a) & (c) to achieve the desired droplet diameter.

### 3.3 Tuning droplet polydispersity

Geometric parameter sensitivity for droplet polydispersity at different flow conditions obtained from ANOVA are shown in Fig. 6. (a). All the geometric parameters were effective in determining droplet polydispersity. However, orifice width and expansion ratio were the dominant parameters in defining polydispersity at low capillary numbers (i.e., $Ca. < 0.14$). At moderate capillary numbers ($Ca. = 0.14 - 0.3$) oil inlet width played an important role in

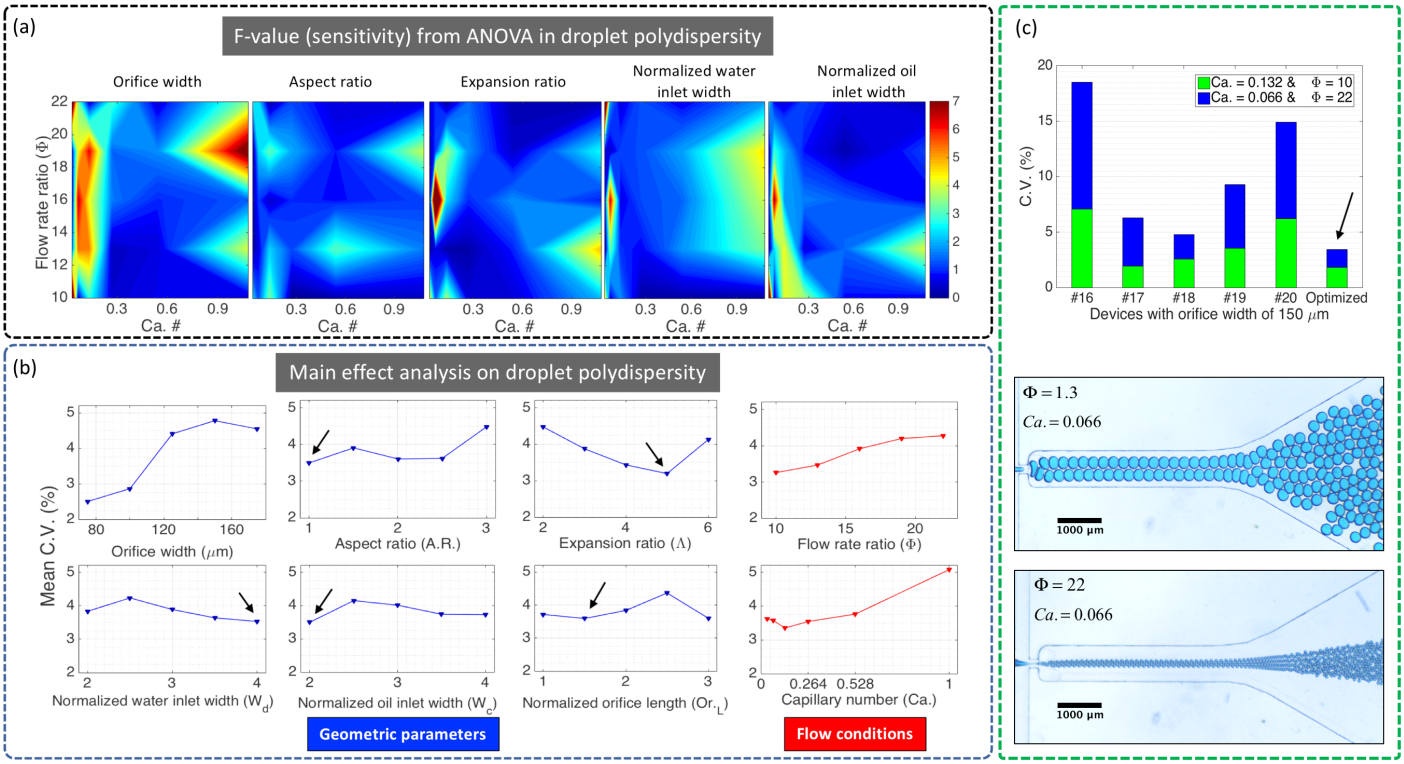


**Fig. 6** Reducing the orifice width was observed to enhance droplet monodispersity. However, if reducing the orifice width is not an available option (i.e., fabrication or design limit) researchers can use the optimum geometric parameters provided here to reduce droplet polydispersity. (a) A heat-map of sensitivity variation of droplet polydispersity to each geometric parameter at different flow conditions. Although orifice width is the dominant geometric parameter in droplet polydispersity, we did not observe a conclusive trend in sensitivity variation. Other parameters also play a role in defining polydispersity at different flow conditions. (b) Main effect plots indicating how variations in parameters affect droplet polydispersity for both geometric parameters (blue) and flow conditions (red). Each plot shows how altering a parameter affects droplet polydispersity. Geometric parameters that result in a minimum polydispersity on average are also indicated by an arrow. (c) To verify the findings in (b) a device with the optimal geometric parameters indicated by arrows in (b) while keeping the orifice size at 150 $\mu$m, that should result in the least polydispersity in comparison to other devices with the same orifice width, was fabricated. The optimized device delivered monodisperse ($C.V. < 2\%$) droplet generation over a wide range of capillary numbers and flow rate ratios.

droplet polydispersity. At high capillary numbers (i.e., $Ca. > 0.5$), although all parameters were important in determining polydispersity, the effects of orifice width and water inlet width were more pronounced than the other parameters. However, we did not observe a conclusive trend on how the significance of each parameter varied as we changed the flow conditions. The main effect plots of 750 experiments for droplet polydispersity are given in Fig. 6. (b). Increasing the orifice width, flow rate ratio, aspect ratio, and capillary number induced more size variation in the formed droplets, thus larger values of $C.V.$ were observed. The main effect plots for the orifice length and normalized water inlet width were inconclusive. However, a weak dependence can be observed, where increasing water inlet width and decreasing orifice length overall results in a reduced polydispersity. The optimum levels of geometric parameters that on average resulted in a lower droplet polydispersity are indicated by black arrows in Fig. 6. (b). To verify these findings, we fabricated a device with an orifice width of 150 $\mu$m (i.e., the orifice width that on average resulted in the highest polydispersity) while keeping the other geometric parameters at their optimum values as shown in Fig. 6. (b). We observed monodisperse ( i.e., $C.V. < 2\%$) droplet generation over a range of capillary numbers and flow rate ratios. We then compared the optimized device observed droplet polydispersity to the other devices with the same orifice width. Polydispersity comparison of the five devices from the original design of experiments with the same orifice size (i.e., $Or. = 150$ $\mu$m), and the optimized device at the same flow conditions are given in Fig. 6. (c). The optimized device produced droplets with a lower $C.V.$ in comparison to the other devices with the same orifice width. Snapshots of monodisperse droplet generation at $Ca. = 0.066$ with two flow rate ratios ($\Phi = 1.3$ & $\Phi = 22$) are shown in Fig. 6. (c).

### 3.4 Tuning generation regime

Most droplet-based applications require monodisperse droplet production.[37] The dripping regime, in general, results in a reduced polydispersity in comparison to the jetting regime. Therefore, keeping the droplet formation regime at the dripping regime preferred in most cases. We studied how altering a geometric parameter or a flow condition affects the droplet formation regime while keeping other parameters constant. Droplet formation at low capillary numbers (i.e., $Ca. < 0.1$) was observed to only occur through the dripping regime regardless of the geometry of the device. Additionally, only jetting regime was observed at high capillary numbers (i.e., $Ca. > 0.5$) independent of the flow-focusing

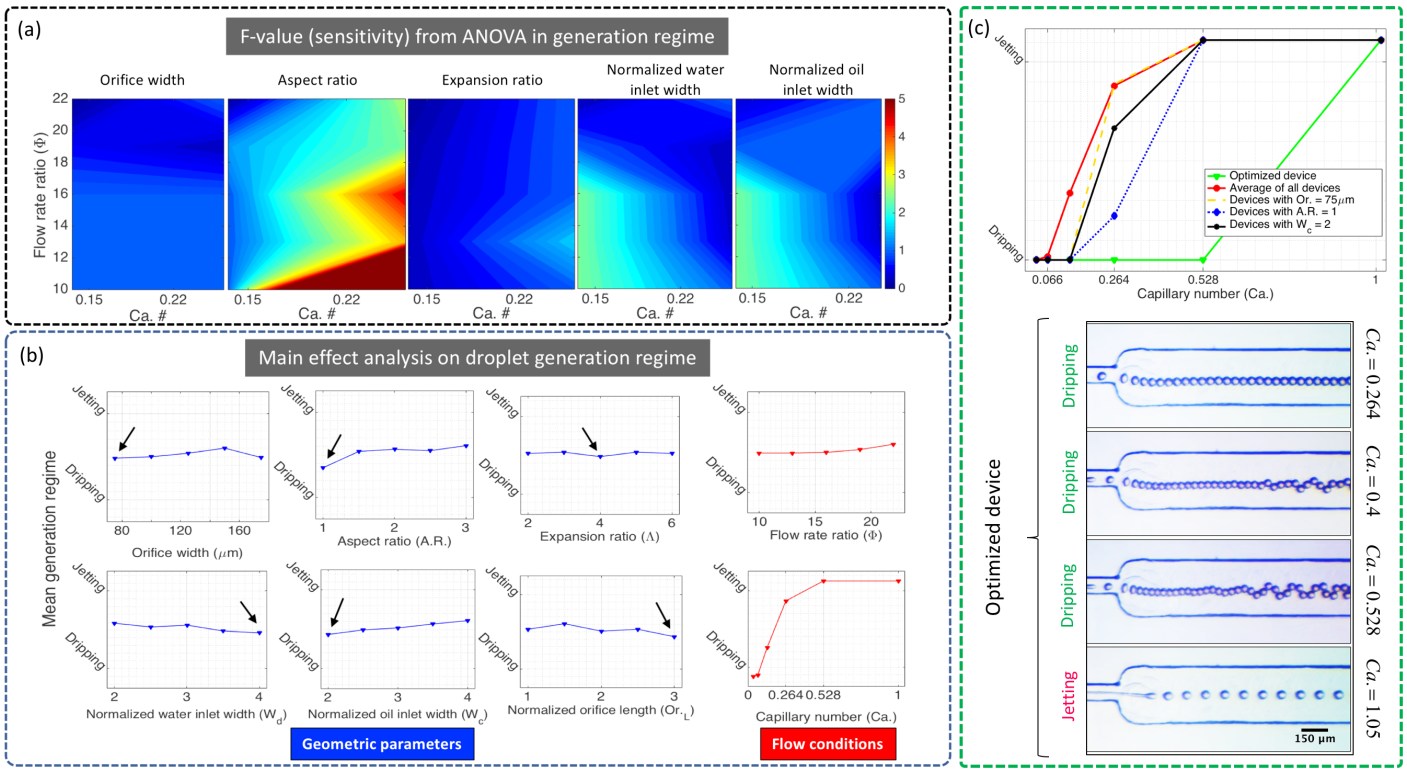


**Fig. 7** A framework that researchers can use to manipulate droplet formation regime to ensure regime change is delayed to a higher capillary number, thus, producing smaller and monodisperse droplets. (a) A heat-map of sensitivity variation of droplet generation regime to each geometric parameter at different flow conditions. At low capillary numbers ($Ca. < 0.1$) droplets were formed at dripping regime. At high capillary numbers ($Ca. > 0.5$) only jetting regime was observed. Therefore, the heat-map is only shown for medium capillary numbers ($Ca. = 0.13 - 0.26$) where a dependence of generation regime on geometry was observed. Aspect ratio, followed by water and oil inlet width are the dominant parameters in determining the droplet formation regime. (b) Main effect plots indicating how altering parameters affect droplet formation regime for both geometric parameters (blue) and flow conditions (red). Each plot shows how altering a parameter affects droplet polydispersity. Often, dripping regime due to a lower polydispersity is more desirable compared to jetting regime. Geometric parameters that result in a higher chance of dripping droplet formation regime at medium capillary numbers are indicated by arrows. (c) A new device with optimal geometric parameters shown by arrows in (b) that should delay the regime change to a higher capillary number was fabricated. As expected, regime change from dripping to jetting in this optimized device happened at a higher capillary number in comparison to the other devices.

geometry. Therefore, in Fig. 7. (a) generation regime sensitivity to the geometric parameters are given only for moderate capillary numbers (i.e., $Ca. = 0.13 - 0.26$) where a dependence of generation regime on geometry was observed. At capillary numbers of $Ca. < 0.14$ normalized water inlet width and normalized oil inlet width were the key parameters in dictating the generation regime. At capillary numbers of $Ca. > 0.14$ aspect ratio became the dominant parameter affecting generation regime. Furthermore, generation regime did not show a strong dependence on the orifice width and expansion ratio. However, expansion ratio was observed to become more effective in dictating the generation regime at higher capillary numbers. Therefore, it can be concluded that aspect ratio is the coarse-tuner and normalized water and oil inlet widths are the fine-tuners in controlling the droplet generation regime. After establishing the key parameters in droplet formation regime, we utilized the main effect analysis to clarify whether changing the geometric parameters, capillary number, and flow rate ratio result in a delayed or advanced regime change (i.e., at higher capillary numbers or at lower capillary numbers). The main effect plots of 750 experiments for generation regime are given in Figure 7. (b). Capillary number was the primary parameter dictating the generation regime. On average, we observed regime change from dripping to jetting to occur at capillary numbers between 0.13 and 0.26 depending on the geometry of the device and the flow rate ratio. We observed that a larger orifice width, aspect ratio, normalized oil inlet width, and flow rate ratio facilitate a regime change from dripping to jetting regime at lower capillary numbers. On the other hand, increasing normalized water inlet width resulted in a delayed regime change (i.e., regime change occurs at higher capillary numbers). Also, a negligible dependency on orifice length and expansion ratio was observed. To verify the finding of this section on controlling the generation regime, we fabricated a new device with optimal geometric parameters shown by arrows in Fig. 7. (b) in order to delay regime change from dripping to jetting to a higher capillary number. For the optimized device, the droplet formation regime change was observed to occur between $Ca. = 0.5 - 1$, which was a higher capillary number than any other device in this study. Fig. 7. (c) compares the average droplet generation regime at a constant flow rate ratio ($\Phi = 16$) among the optimized device, the 25 orthogonal devices, the ones with an orifice width of 75 $\mu$m, devices with an aspect ratio of $A.R. = 1$, and all the geometries with a

normalized oil inlet width of $\overline{W_c} = 2$. As clarified in Fig. 7. (c) the set of devices with an aspect ratio of $A.R. = 1$ showed the closest behavior to the optimized device, which verified that aspect ratio is the primary geometric parameter in dictating droplet formation regime, at a constant flow condition, as previously shown in Fig. 7. (a).

## 4 Discussion

Microfluidic droplet generation was first introduced almost two decades ago.[7] Still, a complete understanding of the governing physics is lacking.[12] The large multidimensional space of flow-focusing droplet generation prevented the field from using non-specific scaling laws to predict droplet size, generation rate, and generation regime.[38] A complex velocity field and a deformable fluid interface made general analytical solutions not feasible. Additionally, numerical solutions for multiphase flows are susceptible to inaccuracies and are computationally costly.[39] Therefore, experimental characterization of droplet generation is the most viable option to improve the current understanding of the field. However, due to the high fabrication costs most of the previous studies focused on flow conditions and fluid properties, with few exceptions.[10,12] Studies with an emphasis on fluid properties and flow conditions are often based on dimensionless numbers specifically capillary number. The capillary number which encapsulates geometry, flow conditions, and fluid properties is a powerful tool to predict and describe the behavior of a droplet generator. However, as demonstrated here capillary number alone is not sufficient to predict the performance of droplet generation. On the other hand, studies that consider geometric variations either lack a thorough geometric design space or do not consider all the performance metrics of droplet generation.[10,12]

Therefore, by exploring a relatively large geometrical design space we characterized the effect of all geometric parameters while considering the flow condition in terms of capillary number and flow rate ratio. We identified the primary and secondary geometric parameters that affect the performance of droplet formation over a wide range of flow conditions. The effect of geometry and flow condition was quantified by providing an average performance change induced by altering all the effective parameters. It was shown that geometry and flow conditions should always be considered simultaneously when predicting performance change caused by either group of parameters. For instance, at low capillary numbers (i.e., the dripping regime) expansion ratio has a negligible effect on droplet size, whereas, at high capillary numbers (i.e., the jetting regime) increasing expansion ratio results in larger droplets. Also, increasing capillary number at low capillary numbers results in the production of smaller droplets, while, increasing capillary number at high capillary numbers has a negligible effect on droplet size. In addition, the effect of expansion ratio on generation rate at low capillary numbers is negligible. However, expansion ratio is the most dominant parameter in determining the generation rate at high capillary numbers.

In addition to characterizing the effect of geometry, flow conditions, and their secondary interactions, the results of this study provide researchers with an easy to use and interpret framework to tune the performance of droplet generators in fewer design iterations by making quantitative and informed decisions. An example use case of this framework is given in the supplementary information section S. 8 where researchers can navigate through and use the information provided in this manuscript to fine tune the droplet size to achieve the desired droplet diameter with fewer design iterations. Similar algorithms could be used to fine tune generation rate, droplet polydispersity, generation regime, or all metrics simultaneously. Aside from geometry and flow conditions, fluid and surface properties also play a major role in determining the performance of droplet generation. Several studies in the literature have reported the effects of viscosity,[40–42] surface tension,[38,43] and surface properties on the behavior of droplet formation and stability.[44,45] In general, a more viscous continuous phase results in smaller droplets and the addition of surfactants (i.e., lower surface tension) results in smaller droplets with higher frequency of generation.[46]

Finally, despite the low cost (i.e., < \$10), these tunable polycarbonate-based microfluidic droplet generators are biocompatible[47,48] and do not require surface treatment to produce monodispersed and stable droplets as demonstrated here. As a result, this framework enables cost-effective and accessible to all droplet-based microfluidics that can be adopted by the life-sciences research groups with limited access to high-end microfabrication facilities. Additionally, characterizing the design space of droplet formation and generating a relatively large dataset of experimental data points enable machine learning tools to be implemented in the field that would result in developing design automation tools for droplet-based microfluidics.[49] This could potentially lead to a new era microfluidic automation where the desired performance is specified by the user and the required geometry and flow conditions are provided by a machine learning tool.

## 5 Conclusions

We proposed a framework to address the challenge of fine-tuning the performance of microfluidic droplet generators to deliver monodisperse droplets at a desired size and rate with fewer design iterations. Flow-focusing droplet generation was studied at a wide range of capillary numbers ($Ca. = 0.03 - 1$) and flow rate ratios (i.e., $10 - 22$) that includes both dripping and jetting droplet formation regimes. Using the Taguchi method, six geometric parameters were varied with five levels for each parameter to fabricate 25 orthogonal devices through a low-cost method. The primary (i.e., coarse tuners) and the secondary parameters (i.e., fine tuners) in dictating droplet formation performance at 30 different flow conditions were identified. It was observed that performance sensitivity to each parameter varies as the flow conditions (i.e., capillary number and flow rate ratio) change. Therefore, using ANOVA method, F-values that represent the sensitivity of all performance metrics to each geometric parameter were provided. Additionally, by conducting the main effect analysis, we presented how altering both geometric parameters and flow conditions changes each performance metric. Through this framework, we were able to fabricate droplet generators that produce monodisperse droplets over a wide range of diameters and generation rates (i.e., $30 - 400$ $\mu$m, and $0.5 - 800$ Hz., respectively)

while each device costs less than $10. Additionally, in the supplementary information we provided 150 experimental data points and a table that allows researchers to choose a device depending on the desired range of droplet diameter and generation rate, then, further tune the device of interest to achieve the desired performance.

## 6 Supplementary information

The supplementary information includes a detailed description of the fabrication and assembly process of the microfluidic devices. Additionally, extra main effect analysis graphs that could be used to tune the performance of droplet generators based on the observed droplet formation regime are given. More information on the role of aspect ratio on the droplet formation regime is provided. 150 experimental data points of droplet diameter and generation rate, alongside with the geometry and flow-conditions that resulted in the observed data point. Finally, a table that provides all of the possible candidates out of the 25 orthogonal devices that could be used to reach a certain range of performance within the observed range of data (i.e., $30-400$ $\mu$m for droplet diameter and $0.5-800$ Hz. for generation rate) is given.

## Conflicts of interest

There are no conflicts to declare.

## Acknowledgements

We would like to thank Dr. Allyson Sgro and Dr. Achini Opathalage at Boston University for their guidance on improving the sealing of the devices and valuable feedback on this research. We are thankful to Marilene Pavan Rodrigues the DAMP lab manager at Boston University. We also thank Radhakrishna Sanka for providing feedback on the manuscript and Rohin Banerji for taking photos of the microfluidic devices. We are grateful to the 2016, 2017 and 2018 Boston University iGEM teams for helping to vet the low-cost microfluidic design tools and techniques developed in the DAMP Lab. This work was supported by the NSF Living Computing Project Award #1522074.

## Notes and references

1 Y.-C. Tan, J. S. Fisher, A. I. Lee, V. Cristini and A. P. Lee, *Lab on a Chip*, 2004, **4**, 292–298.
2 P. Tirandazi and C. H. Hidrovo, *Journal of Micromechanics and Microengineering*, 2017, **27**, 075020.
3 T. Schneider, J. Kreutz and D. T. Chiu, *Analytical chemistry*, 2013, **85**, 3476–3482.
4 H. Song, D. L. Chen and R. F. Ismagilov, *Angewandte chemie international edition*, 2006, **45**, 7336–7356.
5 M. Joanicot and A. Ajdari, *Science*, 2005, **309**, 887–888.
6 C. Rivet, H. Lee, A. Hirsch, S. Hamilton and H. Lu, *Chemical Engineering Science*, 2011, **66**, 1490–1507.
7 T. Thorsen, R. W. Roberts, F. H. Arnold and S. R. Quake, *Physical review letters*, 2001, **86**, 4163.
8 Y.-C. Tan, J. Collins and A. P. Lee, *Micro TAS, Lake Tahoe*, 2003.
9 S. L. Anna, N. Bontoux and H. A. Stone, *Applied physics letters*, 2003, **82**, 364–366.
10 S. Wiedemeier, M. Eichler, R. Römer, A. Grodrian, K. Lemke, K. Nagel, C.-P. Klages and G. Gastrock, *Engineering in life sciences*, 2017, **17**, 1271–1280.
11 S. Xu, Z. Nie, M. Seo, P. Lewis, E. Kumacheva, H. A. Stone, P. Garstecki, D. B. Weibel, I. Gitlin and G. M. Whitesides, *Angewandte Chemie*, 2005, **117**, 734–738.
12 W. Lee, L. M. Walker and S. L. Anna, *Physics of Fluids*, 2009, **21**, 032103.
13 T. Fu, Y. Wu, Y. Ma and H. Z. Li, *Chemical engineering science*, 2012, **84**, 207–217.
14 Z. Liu, J. Zhao, Y. Pang and X. Wang, *Microfluidics and Nanofluidics*, 2018, **22**, 124.
15 J.-C. Baret, O. J. Miller, V. Taly, M. Ryckelynck, A. El-Harrak, L. Frenz, C. Rick, M. L. Samuels, J. B. Hutchison, J. J. Agresti *et al.*, *Lab on a Chip*, 2009, **9**, 1850–1858.
16 Y. Li, G. Liu, J. Xu, K. Wang and G. Luo, *RSC Advances*, 2015, **5**, 27356–27364.
17 A. Vansteene, J.-P. Jasmin, S. Cavadias, C. Mariet and G. Cote, *Microfluidics and Nanofluidics*, 2018, **22**, 61.
18 M. Rasouli, A. A. Mehrizi, M. Goharimanesh, A. Lashkaripour and S. R. Bazaz, *Chemical Engineering and Processing-Process Intensification*, 2018, **132**, 175–186.
19 S. R. Bazaz, A. A. Mehrizi, S. Ghorbani, S. Vasilescu, M. Asadnia and M. E. Warkiani, *RSC Advances*, 2018, **8**, 33103–33120.
20 M. Wörner, *Microfluidics and nanofluidics*, 2012, **12**, 841–886.
21 P. K. Yuen and V. N. Goral, *Lab on a Chip*, 2010, **10**, 384–387.
22 S. A. Aghvami, A. Opathalage, Z. Zhang, M. Ludwig, M. Heymann, M. Norton, N. Wilkins and S. Fraden, *Sensors and Actuators B: Chemical*, 2017, **247**, 940–949.
23 A. Lashkaripour, R. Silva and D. Densmore, *Microfluidics and Nanofluidics*, 2018, **22**, 31.
24 G. Taguchi, *Introduction to quality engineering: designing quality into products and processes*, 1986.
25 S. L. Anna and H. C. Mayer, *Physics of Fluids*, 2006, **18**, 121512.
26 L. Wang, W. Liu, S. Li, T. Liu, X. Yan, Y. Shi, Z. Cheng and C. Chen, *Microsystem Technologies*, 2016, **22**, 677–686.
27 J. Steigert, S. Haeberle, T. Brenner, C. Müller, C. Steinert, P. Koltay, N. Gottschlich, H. Reinecke, J. Rühe, R. Zengerle *et al.*, *Journal of Micromechanics and Microengineering*, 2007, **17**, 333.
28 C.-W. Tsao and D. L. DeVoe, *Microfluidics and nanofluidics*, 2009, **6**, 1–16.
29 A. Kalantarifard, E. A. Haghighi and C. Elbuken, *Chemical Engineering Science*, 2018, **178**, 238–247.
30 P. S. Dittrich, M. Jahnz and P. Schwille, *ChemBioChem*, 2005, **6**, 811–814.
31 J. Canny, *IEEE Transactions on pattern analysis and machine intelligence*, 1986, 679–698.
32 S. Suzuki *et al.*, *Computer vision, graphics, and image processing*, 1985, **30**, 32–46.
33 J. Sklansky, *Pattern Recognition Letters*, 1982, **1**, 79–83.

34 G. R. Iversen, A. R. Wildt, H. Norpoth and H. P. Norpoth, *Analysis of variance*, Sage, 1987.

35 S. Addelman, *Technometrics*, 1962, **4**, 21–46.

36 S. Addelman and O. Kempthorne, *Orthogonal main-effect plans*, Iowa state univ iowa city technical report, 1961.

37 S. Utech, R. Prodanovic, A. S. Mao, R. Ostafe, D. J. Mooney and D. A. Weitz, *Advanced healthcare materials*, 2015, **4**, 1628–1633.

38 C. N. Baroud, F. Gallaire and R. Dangla, *Lab on a Chip*, 2010, **10**, 2032–2045.

39 S. L. Anna, *Annual Review of Fluid Mechanics*, 2016, **48**, 285–309.

40 Y. Gai, J. W. Khor and S. K. Tang, *Lab on a Chip*, 2016, **16**, 3058–3064.

41 J. D. Tice, A. D. Lyon and R. F. Ismagilov, *Analytica chimica acta*, 2004, **507**, 73–77.

42 Z. Nie, M. Seo, S. Xu, P. C. Lewis, M. Mok, E. Kumacheva, G. M. Whitesides, P. Garstecki and H. A. Stone, *Microfluidics and Nanofluidics*, 2008, **5**, 585–594.

43 J.-C. Baret, *Lab on a Chip*, 2012, **12**, 422–433.

44 V. Barbier, M. Tatoulian, H. Li, F. Arefi-Khonsari, A. Ajdari and P. Tabeling, *Langmuir*, 2006, **22**, 5230–5232.

45 W. Li, Z. Nie, H. Zhang, C. Paquet, M. Seo, P. Garstecki and E. Kumacheva, *Langmuir*, 2007, **23**, 8010–8014.

46 N.-T. Nguyen, S. Lassemono and F. A. Chollet, *Sensors and actuators B: Chemical*, 2006, **117**, 431–436.

47 P. M. van Midwoud, A. Janse, M. T. Merema, G. M. Groothuis and E. Verpoorte, *Analytical chemistry*, 2012, **84**, 3938–3944.

48 A. Alrifaiy, O. A. Lindahl and K. Ramser, *Polymers*, 2012, **4**, 1349–1398.

49 A. Lashkaripour, M. Goharimanesh, A. A. Mehrizi and D. Densmore, *Microelectronics Journal*, 2018, **78**, 73–80.

We explored a large design space to identify the coarse/fine tuners in determining droplet size, generation rate, regime, and polydispersity.